aGuangxi Engineering Center in Biomedical Materials for Tissue and Organ Regeneration & Guangxi Collaborative Innovation Center for Biomedicine, The First Affiliated Hospital of Guangxi Medical University, Guangxi Medical University, Nanning, People's Republic of China; bDepartment of Spine Osteopathia, The First Affiliated Hospital of Guangxi Medical University, Guangxi Medical University, Nanning, People's Republic of China; cDepartment of Bone and Joint Surgery, The First Affiliated Hospital of Guangxi Medical University, Guangxi Medical University, Nanning, People's Republic of China; dDepartment of Orthopaedics Trauma and Hand Surgery, The First Affiliated Hospital of Guangxi Medical University, Guangxi Medical University, Nanning, People's Republic of China; eNational Engineering Research Center for Biomaterials, Sichuan University, Chengdu, People's Republic of China

*Contributed equally.

Correspondence: Maolin He, M.D., Department of Spine Osteopathia, The First Affiliated Hospital of Guangxi Medical University, Guangxi Medical University, Nanning 530021, People's Republic of China. Telephone: 86-07715350189; e-mail: 274783289@qq.com; or Jinmin Zhao, M.D., Guangxi Engineering Center in Biomedical Materials for Tissue and Organ Regeneration & Guangxi Collaborative Innovation Center for Biomedicine, The First Affiliated Hospital of Guangxi Medical University, Guangxi Medical University, Nanning 530021, People's Republic of China. Telephone: 86-07715350189; e-mail: zhaojinmin@126.com; or Li Zheng, M.D., Guangxi Engineering Center in Biomedical Materials for Tissue and Organ Regeneration & Guangxi Collaborative Innovation Center for Biomedicine, The First Affiliated Hospital of Guangxi Medical University, Guangxi Medical University, Nanning 530021, People's Republic of China. Telephone: 86-07715358132; e-mail: zhengli224@163.com

Bioconjugated Carbon Dots for Delivery of si*Tnfα* to Enhance Chondrogenesis of Mesenchymal Stem Cells by Suppression of Inflammation

JIANWEI LIU,[a,b,*] TONGMENG JIANG,[a,c,*] CHUN LI,[b,*] YANG WU,[d] MAOLIN HE,[b] JINMIN ZHAO,[a,b,c,d] LI ZHENG,[a] XINGDONG ZHANG[e]

Key Words. Carbon dots • *Tnfα* • Mesenchymal stem cell • Chondrogenesis • Inflammation

ABSTRACT

Although a promising strategy, the mesenchymal stem cell (MSC)-based therapy of cartilage defects is sometimes accompanied with chronic inflammation during the remodeling status, which may hinder cartilage regeneration. During this process, the inflammatory cytokine tumor necrosis factor α (TNFα) plays an important role and may be a potential target. In this study, we investigated the effect of *Tnfα* RNA interference by introducing a functional and highly safe carbon dot (CD)-SMCC nanovector synthesized by bioconjugation of CDs with a protein crosslinker, sulfosuccinimidyl-4-(N-maleimidomethyl) cyclohexane-1-carboxylate (sulfo-SMCC), as the vehicle of the silenced TNFα (si*Tnfα*) on chondrogenesis of MSCs. The results showed that CD-SMCC displayed intense fluorescence with well-dispersed and positively charged properties, which favored effective binding and delivering of si*Tnfα* into the MSCs. CD-SMCC-si*Tnfα* nanoformula also exhibited considerably high transfection efficiency and nearly no cytotoxicity, which is preferred over commercial polyethyleneimine. Interference of *Tnfα* by CD-SMCC-si*Tnfα* markedly promoted the chondrogenesis of MSCs, as indicated by upregulating cartilage-specific markers. Furthermore, in vivo exploration indicated that CD-SMCC-si*Tnfα* transfected MSCs accelerated cartilage regeneration. In conclusion, this study demonstrated that in combination with the novel CD-SMCC nanovector, targeting *Tnfα* may facilitate stem cell-based therapy of cartilage defects. STEM CELLS TRANSLATIONAL MEDICINE 2019;8:724–736

SIGNIFICANCE STATEMENT

This study developed a functional and highly safe CD-SMCC nanovector synthesized by bioconjugation of carbon dots (CDs) with a protein crosslinker, sulfosuccinimidyl-4-(N-maleimidomethyl) cyclohexane-1-carboxylate (sulfo-SMCC), which displayed intense fluorescence with well dispersed and positive-charged properties favorable for effective binding and delivering of small interfering RNA. It was found that interference of Tnfα by CD-SMCC-siTnfα markedly promoted the chondrogenesis of MSCs, which is preferred over commercial polyethyleneimine. The study demonstrated that Tnfα may be a potential target and, in combination with the novel CD-SMCC nanovector, is promising for stem cell-based therapy of cartilage defects.

INTRODUCTION

Mesenchymal stem cells (MSCs) have recently attracted much attention as sources for the clinical therapy of a variety of diseases [1, 2], including cartilage injury, due to their ease of expansion and wide range of functions [3, 4]. Recruited MSCs can be specifically induced along the chondrogenic lineage in the presence of specific growth factors, molecules, and epigenetic modifications. However, the immune modulation capability of MSCs is somehow suppressed by chronic inflammation [5] during regeneration

[6], which impairs the chondrogenesis of MSCs and restrains the major constituent of the cartilage matrix (type II collagen), thus remaining a challenge for MSC therapy of cartilage defects.

Notably, tumor necrosis factor-α (TNFα) is one of the proinflammatory cytokines mediating local inflammatory processes in the joint and has an inhibitory effect on chondrogenesis. Elevated TNFα is detected in synovial tissue and fluid during the cartilage destruction cascade [7], which suppresses the synthesis of cartilage matrix (e.g., aggrecan and type II collagen) [8, 9]. The potential mechanism may involve TNFα that
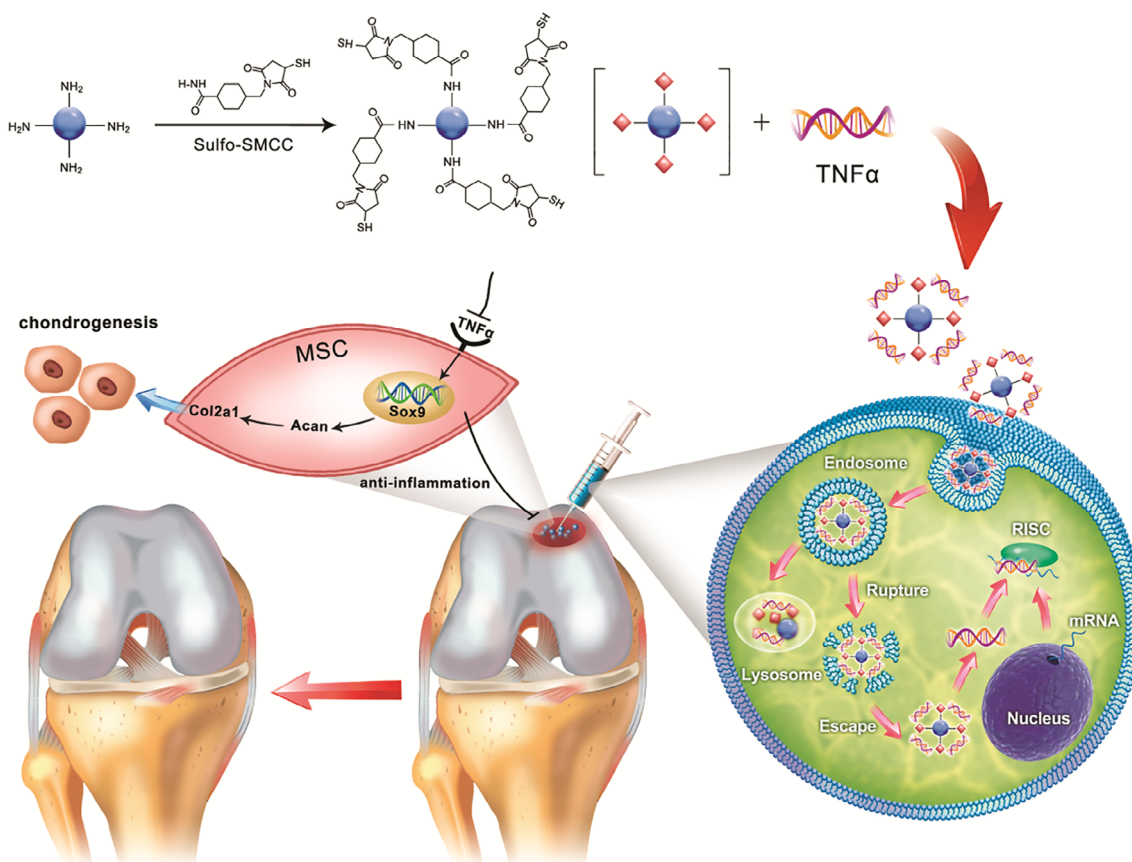
Figure 1. Schematic illustration of the formation of carbon dot (CD)-succinimidyl-4-(N-maleimidomethyl) cyclohexane-1-carboxylate-silenced TNFα complexes and the CD-based nanocarrier for gene delivery and real-time monitoring of cellular trafficking in vitro and in vivo for enhancing cartilage repair.

activates a transcription factor, NF-κB, which in turn inhibits the synthesis of SOX9, which is a crucial transcription factor required for chondrogenic differentiation [10, 11]. TNFα also induces cell apoptosis in chondrocytes [12] and inhibits the migration of chondrogenic progenitor cells from nonfibrillated osteoarthritic cartilage [13]. Interference of TNFα obviously eases cartilage degeneration and promotes cartilage regeneration in post-traumatic arthritis [14, 15]. These findings suggest that TNFα may influence chondrogenic differentiation and may be one of the potential targets for MSC therapy. mRNA silencing of TNFα in MSCs by using small interfering RNA (siRNA)-mediated RNA interference (RNAi) may enhance chondrogenesis.

Successful gene delivery requires that the vehicles have favorable biocompatibility to avoid the elicitation of an adverse host immune response, as well as high transfection efficiency. Among the various vehicles, nanoparticles have attracted the most attention due to their unique properties, including as biosafety, flexibility, ease of formulation, and high delivery efficiency [16]. Among the various carriers, quantum dots (QDs) and carbon dot (CD)-based gene delivery systems are two of the most widely used fluorescent delivery systems [17, 18]. In a previous study, we reported on QD nanovectors modified by sulfosuccinimidyl-4-(N-maleimidomethyl) cyclohexane-1-carboxylate (sulfo-SMCC) for gene delivery and gene targeting in MSCs [19]. Although efficient in gene silencing, the heavy metal toxicity of QDs hinders its application to gene therapy in vivo

[20]. Another fluorescent nanomaterial with both favorable biocompatibility and monodispersity, CDs have been proven to be excellent and efficient gene delivery vectors [21] and may replace QDs as the leading carrier in gene transfer. However, the gene may not bind closely to CDs without optimized surface modification [22]. A previous study from our laboratory demonstrated that QDs bioconjugated with sulfo-SMCC can form a stable thioether bond [19], which retained the integrity of siRNA [23] and greatly increased the transfection efficiency [24]. Sulfo-SMCC contains N-hydroxysuccinimide ester and maleimide groups, allowing stable covalent conjugation of amine-containing and sulfhydryl-containing molecules [25]. This may shed light on the modification of CDs.

Based on our previous study, we synthesized CD-SMCC by bioconjugation of CDs with SMCC for the gene transfer of silenced TNFα (si*Tnfα*) in MSCs to assess the effects of si*Tnfα* on chondrogenic differentiation, with the intention of enhancing chondrogenesis of MSCs and further cartilage regeneration in vivo (Fig. 1). Polyethyleneimine (PEI) was used as the control. This study may provide new insight into cartilage repair.

MATERIALS AND METHODS

Reagents and Chemicals

α-Minimum essential medium (α-MEM, Gibco, Shanghai, China), trypsin, and fetal bovine serum (FBS) were obtained from Gibco

BRL (Invitrogen Co., Carlsbad, CA). PEI (25 kDa) was purchased from Sigma (Shanghai, China). 3-(4,5-Dimethylthiazol-2-yl)-2,5-diphenyltetrazolium bromide (MTT) was obtained from Sigma (St. Louis, MO). Amine functionalized water-soluble CDs were purchased from Janus (Nanjing, China), whereas thiol-modified FAM-labeled siRNAs (*Tnfα*-siRNA sequence: GGU UCU CUU CAA GGG ACA ATT) were purchased from Sangon Biotech (Shanghai, China). Fifty microliters of CDs (10 mg/ml) were diluted with borate buffer to form a 200 μg/ml solution and filtered through a 0.22-μm filter, followed by the addition of 10 μl of sulfo-SMCC (Life Technologies, Shanghai, China) solution. The mixture was incubated and shaken in a thermomixer (Eppendorf, Germany) at 300 rpm for 1 hour at 37°C. A desalting column equilibrated with MES buffer was prepared. After collecting the fluorescent fraction, the activated CD-SMCC was passed through the equilibrated desalting column and eluted with MES after centrifugation to remove aggregates. According to the protocol, the thiol-modified si*Tnfα* was diluted with diethyl pyrocarbonate water to be prepared as a working solution (4 μg/ml). The CD-SMCC-si*Tnfα* complexes at different weight ratios (CD-SMCC to si*Tnfα*) were formulated by blending an equal volume of CD-SMCC solution with the si*Tnfα* solution, which was vortexed for 1 minute. After half an hour, the CD-SMCC-si*Tnfα* complexes were harvested and stored at 4°C for subsequent experiments.

Characterization Studies

The average particle size of the CDs and CD-SMCC-si*Tnfα* complexes were measured by dynamic light scattering (DLS) analysis. CD-SMCC solution was dropped on a cover glass and then analyzed by a fluorescence microscope (BX53, Olympus, Tokyo, Japan) under ultraviolet (UV; 330–385 nm), blue (460–495 nm), and green (530–550 nm) light excitation, respectively. The fluorescence emission spectra of CD-SMCC were detected using a spectrofluorometer (RF-5301PC, Shimadzu, Japan). UV–visible absorbance spectra of both CDs and CD-SMCC were recorded using a microplate reader (Mutiskan Go, CA). Fourier transform infrared (FT-IR) spectra of both CDs and CD-SMCC were obtained using a SPECTRUM100 Spectrometer (Perkin Elmer, MA) in the frequency range of 500–4,000 cm^{-1}. The zeta potential (surface charge) of the CD-SMCC-si*Tnfα* complex was determined by a Zeta Sizer Nano Z apparatus (Malvern, U.K.).

Gel Electrophoresis

To examine the binding effect of CD-SMCC in gene delivery, an agarose gel retardation study was conducted using CD-SMCC-si*Tnfα* complexes with various weight ratios of 2:1, 5:1, 10:1, 20:1, and 40:1. The samples were loaded on a 1% agarose gel containing ethidium bromide (0.5 μg/ml) after mixing with loading buffer. After running the gel at 90 V for 20 minutes, the gel was imaged with a gel imager (BIO-RAD Laboratories, Hercules, CA).

Cell Culture

The MSCs were flushed from the femur and tibia of rats with a syringe containing 1 ml of phosphate-buffered saline (PBS) and then cultured in α-MEM medium (Gibco) supplemented with 10% FBS, 100 units per milliliter penicillin, and 100 μg/ml streptomycin at 37°C in a 5% CO_2 humidified incubator. The medium was replaced every 3 days, and MSCs of passage 3 were used.

Cytotoxicity of CD-SMCC-si*Tnfα*

To evaluate the cytotoxicity of CD-SMCC-si*Tnfα* complexes, the MTT assay was used. MSCs were seeded in 96-well plates at 5,000 cells per well, and CD-SMCC-si*Tnfα* complexes (20 μl) with varied weight ratios were added in each well. PEI (25 kDa) was used as the control. After 72 hours of incubation, the MTT stock solution was added, followed by a 4-hour incubation at 37°C. Then, the medium was removed, and 200 μl of dimethyl sulfoxide (Gibco) was used to dissolve the formazan product. The absorbance of each well was measured at 570 nm by a microplate reader (Thermo Fisher Scientific, U.K.). All experiments were performed with six replicates.

In Vitro Transfection

1×10^5 MSCs were seeded into each well of 6-well plates. After 24 hours, the complete culture medium was changed to α-MEM without serum and antibiotics. The CD-SMCC-si*Tnfα* complexes with an optimal weight ratio were added in each well. The PEI-si*Tnfα* complexes were used as the control. After incubation for 12 hours, the supernatant was discarded, and the MSCs were rinsed with PBS twice. Then, complete culture medium was added to the MSCs.

Transmission Electron Microscopy Analysis

The morphology of the CDs and CD-SMCC-si*Tnfα* complexes were observed by transmission electron microscopy (TEM; H-7650, Hitachi, Japan) at an accelerating voltage of 200 kV. All samples were dried and analyzed by TEM.

Transfected MSCs by CD-SMCC-si*Tnfα* were also examined by TEM. Briefly, the transfected cells were fixed with 2.5% glutaraldehyde for 4 hours at 4°C and then treated with 1% osmium tetroxide at room temperature. The samples were cut into 60 nm ultrathin sections and mounted onto a copper mesh. The sections were analyzed by TEM (H-7650, Hitachi, Japan).

Confocal Laser Scanning Microscope Analysis

To track the cellular uptake of the CD-SMCC-si*Tnfα* complexes, an assay by confocal laser scanning microscope (CLSM) was used. The MSCs were seeded in a confocal dish at a density of 1×10^5 cells per well. After 24 hours of culture, the medium was replaced by 2.25 ml of FBS-free α-MEM medium, along with 250 μl of the CD-SMCC-si*Tnfα* complexes of optimal dose. After being cultured at 37°C for 2 hours, 4 hours, and 8 hours, the cells were rinsed with PBS three times. Then, all the samples were stained with RedDod1 for 15 minutes and LysoTracker Yellow for 30 minutes in the dark. Confocal images were obtained at each time point using a CLSM (Nikon A1, Japan).

Flow Cytometry

Flow cytometry was used to quantitatively evaluate the transfection efficiency of CD-SMCC-si*Tnfα*. The CD-SMCC-si*Tnfα* complexes of different weight ratios (10:1, 20:1, and 40:1) were added to the 6-well plates preseeded with MSCs of 1×10^5 cells per well. The cells were trypsinized, harvested and then washed with PBS after 6 hours, 12 hours, and 24 hours, respectively. PEI-si*Tnfα* transfected MSCs were also detected. The intracellular FAM fluorescence signals were identified by flow cytometry in a fluorescence-activated cell sorting Canto apparatus (Becton Dickinson, Franklin, NJ).

In Vitro Chondrogenic Induction

Briefly, in vitro chondrogenic induction was performed as previously reported [26]. Chondrogenic inducing medium was based on α-MEM (Gibco) containing 10% FBS, 1% insulin-transferrin-selenium solution (Gibco), 100 nM dexamethasone (Sigma–Aldrich, Billerica, MA), 50 μg/ml ascorbic acid (Sigma), and 10 ng/ml TGF-β1 (Prope Tech, Rocky Hill, NJ). After 7, 14, and 21 days of induction, chondrogenic effects were evaluated by studying GAG content and chondrocytic specific mRNAs identified by PCR.

Measurement of Total DNA and GAG Content

Four groups were investigated, including untreated MSCs (untreated), CD-SMCC transfected MSCs (CD-SMCC), PEI-si$Tnf\alpha$ (PEI-Si), and CD-SMCC-si$Tnf\alpha$ transfected MSCs (CD-SMCC-Si), which were cultured for 7, 14, and 21 days. The samples were fully immersed in 60 μg/ml proteinase K (Sigma) solution for 10 hours at 60°C for digestion, followed by the addition of Hoechst 33258 (Sigma) for 5 minutes. The fluorescence was examined with a microplate fluorescence reader (FLX800, Bio-Tec, Burlington, VT) at 460 nm by using calf thymus DNA as a standard. The total glycosaminoglycan (GAG) production was measured by the 1,9-dimethylmethylene blue (DMMB) colorimetric method [27]. The proteinase K-digested specimens were mixed with DMMB solution and the absorbance value was read in a microplate reader (Thermo, Karlsruhe, Germany) at 525 nm. The amount of GAG production was normalized to the total DNA content to evaluate the biosynthetic activity of the cells in all groups.

Real-Time PCR Analysis

To detect the expression of $Tnf\alpha$ and cartilage-specific genes in transfected MSCs, including aggrecan ($Acan$), $Col2a1$, and SRY-related high mobility group-box gene 9 ($Sox9$), real-time (RT)-PCR analysis was performed. Total RNA was extracted using an RNA isolation kit (Invitrogen Life Technologies), as instructed by the manufacturer. After the reverse transcribed reaction, real-time fluorescent quantitative PCR was detected by the LightCycler[R]96 (Roche, Switzerland). The conditions of RT-PCR were as follows: 40 cycles of 95°C for 10 minutes, 94°C for 15 seconds, and 60°C for 1 minute. All primers (Supporting Information Table S1) were designed based on established GenBank sequences, with β-actin ($Actb$) as an internal control for the assessment of PCR efficiency. Ct values were also determined.

Animal Model

The animal study was approved by the Committee on the Ethics of Animal Experiments of Guangxi Medical University (2017-02-03). The animal experiment conditions were as previously stated (animal experimental statement) [3]. Ten-week-old male SD rats were anesthetized using 2.5% sodium pentobarbital (30 mg/kg). After routine skin preparation, a medial para-patellar skin incision was made, and the knee joint and chondral surface of the femur was fully exposed by lateral dislocation of the patella. By using a punch, a full thickness cylindrical cartilage defect (2.5 mm in diameter, 1.0 mm in depth) was created in the center of the patellar groove. Approximately 0.4 ml of the cell clusters (1×10^5 cells per milliliter) were injected into the defect site. Then, the patella

was carefully relocated, and the incisions were tightly sutured layer by layer. The SD rats were divided into four groups: non-treated MSCs (untreated), CD-SMCC transfected MSCs (CD-SMCC), PEI-si$Tnf\alpha$ transfected MSCs (PEI-Si), and CD-SMCC-si$Tnf\alpha$ transduced MSCs (CD-SMCC-Si). Each group contained eight rats, and the experiments were performed on the bilateral knee joints of each rat.

Macroscopic Observation

After 4 and 8 weeks of therapy, the rats were sacrificed by an intravenous overdose of pentobarbital, and their knee joints were harvested. The knee joints from each group were examined and photographed for evaluation. Finally, the samples were fixed in 4% paraformaldehyde for hematoxylin–eosin (H&E) staining, Safranin-O staining, and immunohistochemistry. The International Cartilage Repair Society (ICRS) macroscopic score was performed [28].

Histological and Immunohistochemical Evaluation

After fixing in paraformaldehyde, the samples were decalcified and embedded in paraffin and cut into 5-μm sections. Paraffin sections were deparaffinized in xylene and hydrated with graded alcohol. H&E and Safranin-O stains were used to evaluate morphology and GAG accumulation of engineered cartilage. The histological score was blindly observed by three independent investigators (S.C., L.Y., and J.T.) using an established histological scoring system [29].

The secretion of type II collagen and TNFα in the regenerated tissue was analyzed with an immunohistochemical staining kit (Bioss, Beijing, China). Briefly, the sections were incubated with 3% H_2O_2 for 10 minutes to exclude endogenous peroxidase activity. Then, the samples were blocked with goat serum for 10 minutes, followed by the incubation of mouse anti-rabbit collagen type II (COL2A1, Acris Antibodies GmbH, AF5710) and TNFα (Boster, Wuhan, China) antibodies with 1:200 dilutions overnight. After incubating with the secondary antibody, the samples were visualized by a 3,3′-diaminobenzidine tetrahydrochloride kit (Boster, Wuhan, China) before brief counterstaining with hematoxylin. Images were viewed under an upright microscope (Olympus BX53, Tokyo, Japan).

Statistical Analysis

Data analyses were performed using SPSS 16.0 and GraphPad 5.0. One-way analysis of variance and Tukey's test were used. The statistically significant value was set at $p < .05$.

Characterization of CD-SMCC-siRNA

The morphology and structure of CDs and CD-SMCC-si$Tnf\alpha$ were explored by TEM. As shown in Figure 2A, 2B, both CDs and CD-SMCC-si$Tnf\alpha$ displayed monodisperse and spherical morphology, with a diameter range of 4–10 nm and 13–22 nm, respectively. Covalent bioconjugation to SMCC-si$Tnf\alpha$ increased the size of the CDs, implying that there existed slight aggregation of nanoparticles during the process of conjugation. Based on the DLS analysis, the average size of CD particles was approximately 7.4 nm ± 1.3 nm (Fig. 2A) and that of CD-SMCC-si$Tnf\alpha$ complexes was 16.1 nm ± 2.8 nm (Fig. 2B), consistent with the results obtained by TEM. These findings revealed that
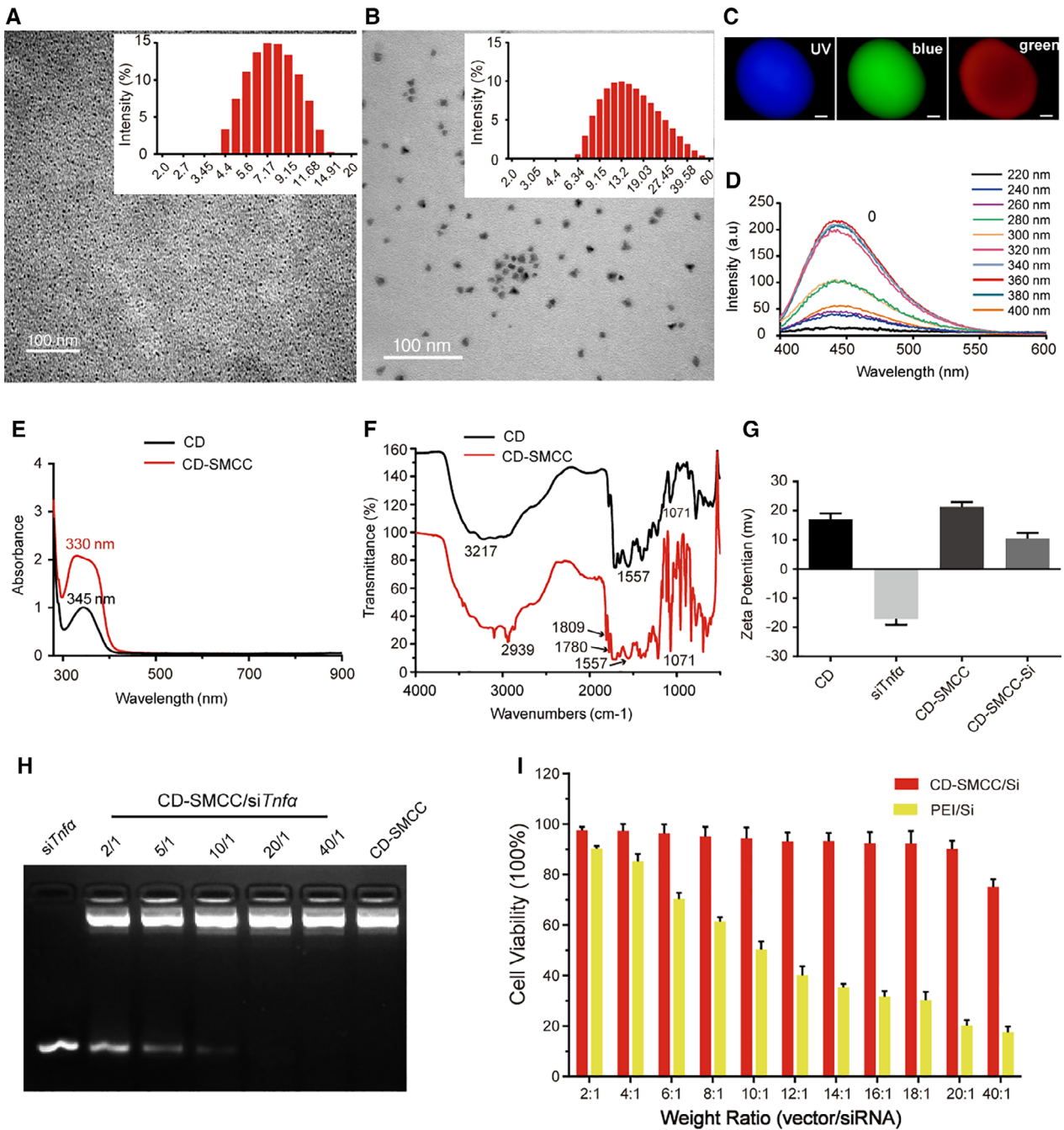
Figure 2. Characterization of carbon dot (CD)-succinimidyl-4-(N-maleimidomethyl) cyclohexane-1-carboxylate (SMCC), as well as the assessment of the CD-loads of small interfering RNAs (siRNAs). **(A):** Transmission electron microscopy (TEM) image (scale bar: 100 nm) and corresponding size distribution of the CDs. **(B):** TEM image (scale bar: 100 nm) and corresponding size distribution of CD-SMCC-silenced TNFα (si*Tnfα*) complexes. **(C):** CD-SMCC solution observed under different excitation wavelengths (scale bar: 400 nm). **(D):** Photoluminescence emission spectra (from 220 nm to 400 nm with a 20 nm increment) of CD-SMCC. **(E):** UV absorption spectrum before and after CDs reaction with SMCC. **(F):** The Fourier transform infrared spectra of the CDs and the CD-SMCC. **(G):** Zeta potential changes in the surface charge. **(H):** The ability of CD-SMCC load of the siRNA was evaluated by agarose gel electrophoresis. Lanes 2–6 correspond to CD-SMCC-siTnfα ratios of 2:1, 5:1, 10:1, 20:1, and 40:1. Lanes 1 and 7 correspond to siTnfα and CD-SMCC. **(I):** The cytotoxicity of CD-SMCC-Si and polyethyleneimine-Si at different weight ratios was assessed by an MTT assay (% viability cells).

CD-SMCC has a potent affinity for macromolecular siRNA, which could protect the RNA from nuclease degradation and assist cellular uptake.

Figure 2C shows that CD-SMCC in solution presented blue, green, and red luminescence, respectively, which demonstrated

that the luminescence property of CDs did not change after modification. The excitation-dependent photoluminescence emission spectra were further used to evaluate the wavelength-dependent feature of CD-SMCC. The excitation wavelengths ranged from 220 nm to 400 nm, with a peak intensity at 360 nm

(Fig. 2D). It has been reported that the different origins of photoluminescence in CDs lead to the differently distributed emission energy traps on the surface [30]. As shown in Figure 2E, the ultraviolet absorption spectrum of CDs was observed at 345 nm. After modification with SMCC, the peak was observed at 330 nm with a minor blueshift, which is due to the $n–\pi^*$ transition of the C$=$O group. FT-IR spectra were further recorded to identify the organic functional groups on SMCC-modified CDs. As shown in Figure 3F, compared with the spectrum of CDs, peaks of CD-SMCC at 2,939 cm^{-1}, 1,809 cm^{-1}, and 1,780 cm^{-1} indicated the presence of C—H, C$=$O and N–H bonds, respectively. Additional —HN—CO bonds in the CD-SMCC group suggested the existence of SMCC. Meanwhile, the CDs and CD-SMCC exhibited similar characteristic peaks at 1,557 and 1,071 cm^{-1}. Both CDs and CD-SMCC-si$Tnf\alpha$ complexes exhibited positive charges by zeta potential measurements, which averaged 17.06 mV $\pm$ 2.3 mV and 21.33 mV $\pm$ 1.4 mV, respectively (Fig. 2G). In contrast, the siRNA surface showed negative charges of -17.13 mV $\pm$ 1.8 mV. The charge reduction (10.05 mV $\pm$ 2.1 mV) of CD-SMCC-si$Tnf\alpha$ indicated successful covalent bioconjugation.

Binding Efficiency of CD-SMCC-siRNA Complexes

It has been generally accepted that naked CDs can hardly be conjugated with dsRNA, which necessitates surface functionalization of CDs [31]. We proposed that the activated CD-SMCC has great potential in binding with siRNA and tested the affinity of CD-SMCC for siRNA with various weight ratios of 2:1, 5:1, 10:1, 20:1, and 40:1 by agarose gel electrophoresis. As shown in Figure 2H, the intensity of the si$Tnf\alpha$ migration bands gradually decreased with the increase in weight ratios. When the ratio was equal to or above 20:1, almost no RNA would migrate toward the anode, demonstrating that the RNA was fully bound to CD-SMCC. These results indicated that CDs activated by SMCC were endowed with excellent complexing ability with siRNA, which is essential for gene delivery.

Cytotoxicity of CD-SMCC-siRNA Complexes

To study the chondrogenic potential of MSCs by immune modulation, the carrier is required to have not only high transfection efficiency but also exceedingly low cytotoxicity to elicit minimal host response. The MTT assay was used to evaluate the cytotoxicity of the CD-SMCC-si$Tnf\alpha$ complexes to rat MSCs, with PEI-si$Tnf\alpha$ as the control. As shown in Figure 2I, the cytotoxicity of CD-SMCC-si$Tnf\alpha$ complexes with different weight ratios from 2:1 to 20:1 was minimal, with more than 90% cell viability. However, cell viability was slightly less when the ratio increased to 40:1. This result implied that the CD-SMCC-si$Tnf\alpha$ complexes had dose-dependent toxicities. In contrast, PEI-si$Tnf\alpha$ with the same weight ratios exhibited noticeable dose-dependent cytotoxicity. Specifically, the cell viability dropped below 70% when the ratio was >6:1. Activated CD-SMCC is advantageous when compared with the conventional commercial transfection reagent PEI, has favorable biocompatibility and may not cause an adverse immune response.

Cellular Uptake of the CD-SMCC-siRNA Complexes by MSCs

To investigate the cellular ultrastructural response to CD-SMCC-si$Tnf\alpha$, transfected MSCs at different time points were detected by TEM. As shown in Figure 3A, 3B, multiple internalized CD-SMCC-si$Tnf\alpha$ clustered onto the surface of the cytomembranes at 2 hours post-transfection, followed by the extension of numerous cellular filopodia toward nanoparticle clusters to wrap them. After 4 hours, most of the endocytosed CD-SMCC-si$Tnf\alpha$ escaped from the cell membrane and aggregated from the early endosomes to the late ones (Fig. 3B, 3C). Eight hours later, they gradually moved closer to the nucleus, where the delivered genes were released (Fig. 3D, 3E). Sometimes, several endosomes were broken, which allowed the discharged CD-SMCC-si$Tnf\alpha$ to enter the cytoplasm (Fig. 3D, 3F). This study confirms the assertion that enveloped nonviral complexes experience endosome escape based on the proton sponge hypothesis [32, 33]. Finally, most of the CD-SMCC-si$Tnf\alpha$ complexes that entered the cells were observed in the cytosol of MSCs after a 12 hours transfection (Fig. 3G). Overall, these findings demonstrated that the CD-SMCC bundled si$Tnf\alpha$ successfully penetrated the endocytosis pathway to reach the cytoplasm and escaped endosome wrapping.

The Transfection Process of CD-SMCC-siRNAs in MSCs

Negatively charged siRNA is easily degraded by nucleases, making it difficult to enter the cells through the cell membrane [30, 34, 35]. A functional nanocomposite formulation can protect siRNAs from degradation [36]. To confirm the protection of active CD-SMCC nanoparticles from siRNA enzymolysis, we studied the cellular internalization of CDs by CLSM. It was observed that large numbers of nanoparticles indicated by blue fluorescence and FAM-si$Tnf\alpha$ (green) were internalized into the cells with RedDod1-labeled nuclei (Fig. 4). At 2 hours post-transfection, CD-SMCC and FAM-si$Tnf\alpha$ assembled around the cell membranes. After 4 hours, most uptaken nanoparticles were present in the endosomal compartments, whereas the green FAM-si$Tnf\alpha$ and the blue CDs were predominantly located in the yellow-labeled organelles, which suggested that the CD-SMCC-si$Tnf\alpha$ complexes were retained in the endosomes or lysosomes. Eight hours later, an increasing number of CDs were distributed at the periphery of the nucleus instead of the organelles, which indicated endosomal escape. During the whole process, green fluorescence by FAM-si$Tnf\alpha$ intensified in a time-dependent manner. These findings mirror the observations from the cellular uptake mechanism of CD-SMCC-si$Tnf\alpha$ by TEM, demonstrating effective transfection. In addition, a remarkable increase in green fluorescence appeared in the cytoplasm, which revealed effective silence and stable expression of siRNA released from CD-SMCC-si$Tnf\alpha$ complexes. This remarkable fluorescent feature endows CD-SMCC with an intrinsic ability for both gene delivery and bioimaging.

Transfection Efficiency of CD-SMCC-siRNA Complexes

Flow cytometry was used to quantitatively measure the transfection efficiency of MSCs. The results showed that only 0.10% of the untreated MSCs were positive, whereas 39.95%, 83.64%, and 64.38% of the MSCs were positive followed by incubation with the CD-SMCC-si$Tnf\alpha$ complexes for 6 hours, 12 hours, and 24 hours, respectively (Fig. 5A). Among the various time points, 12 hours was the best for transfection. For the weight ratios of CD-SMCC-si$Tnf\alpha$ complexes, 20:1 (86.69%) was much higher than 10:1 (53.78%) and 40:1 (63.41%), consistent with the findings by electrophoresis. A higher dose (40:1) inversely led to the decline of transfection efficiency because of the increased cytotoxicity, which was also verified by MTT analysis. Under optimal weight ratios and transfection time (20:1, 12 hours),
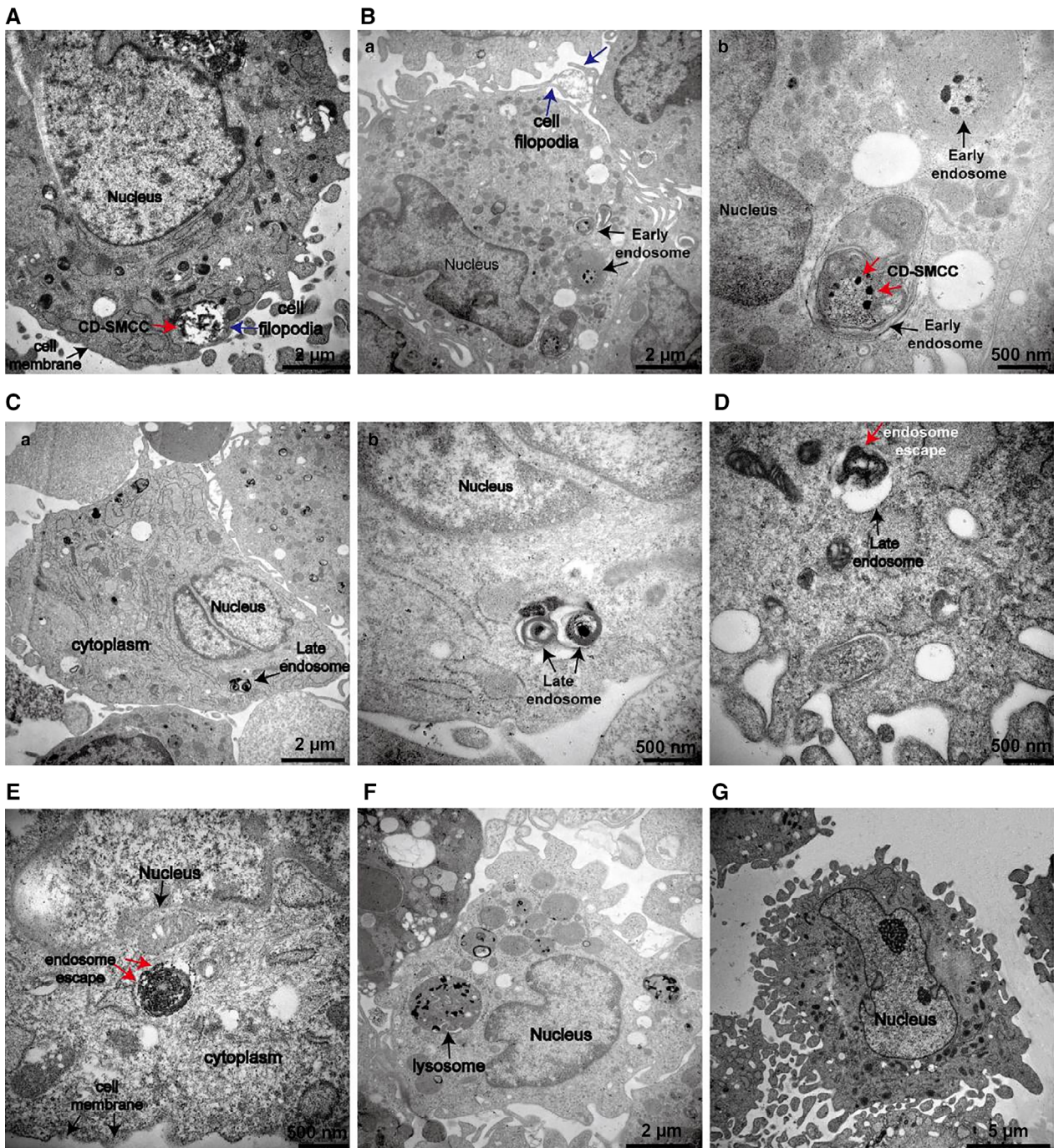
Figure 3. The cellular uptake of carbon dot (CD)-succinimidyl-4-(N-maleimidomethyl) cyclohexane-1-carboxylate (SMCC) bundled small interfering RNAs (siRNAs) as determined by transmission electron microscopy (TEM). **(A, B):** CD-SMCC-silenced TNFα (si*Tnfα*; red arrow) approaching the cell membrane, mesenchymal stem cells (MSCs) stretch out cellular filopodia (blue arrow) and wrapped them. (B): **(Ba):** CD-SMCC-si*Tnfα* clusters were being phagocytized and encapsulated by early endosomes (scale bar: 2 μm) and **(Bb)** are magnifications (scale bar: 500 nm). Black arrows indicate early endosomes and red arrows indicate CD-SMCC-si*Tnfα*. **(C): (Ca):** The late endosomes include CD-SMCC-si*Tnfα* and cell debris dispersed in the cytoplasm (black arrow, scale bar: 2 μm) and (Ca), is magnified in **(Cb**; scale bar: 500 nm). **(D, E):** The endosomes ruptured and CD-SMCC-si*Tnfα* escaped from the endosomes. Endosomes gradually moved close to the nucleus, where the complex genes could be delivered (scale bar: 500 nm). **(F):** TEM image of the lysosome (scale bar: 2 μm). **(G):** Twelve hours after transfection, all of the CD-SMCC-si*Tnfα* complexes entered the cells (scale bar: 5 μm).

87.93% of the MSCs administered CD-SMCC-si*Tnfα* were positive, which was markedly higher than those administered PEI-si*Tnfα* (69.89%). The transfection efficiency of the CD-SMCC-siRNA was higher than commercial PEI, which may be due to the small particle size of CDs and the aggregation effects when combined with the siRNA to prevent enzymolysis [37]. The result demonstrated that CD-SMCC was a safe vector with high efficiency.
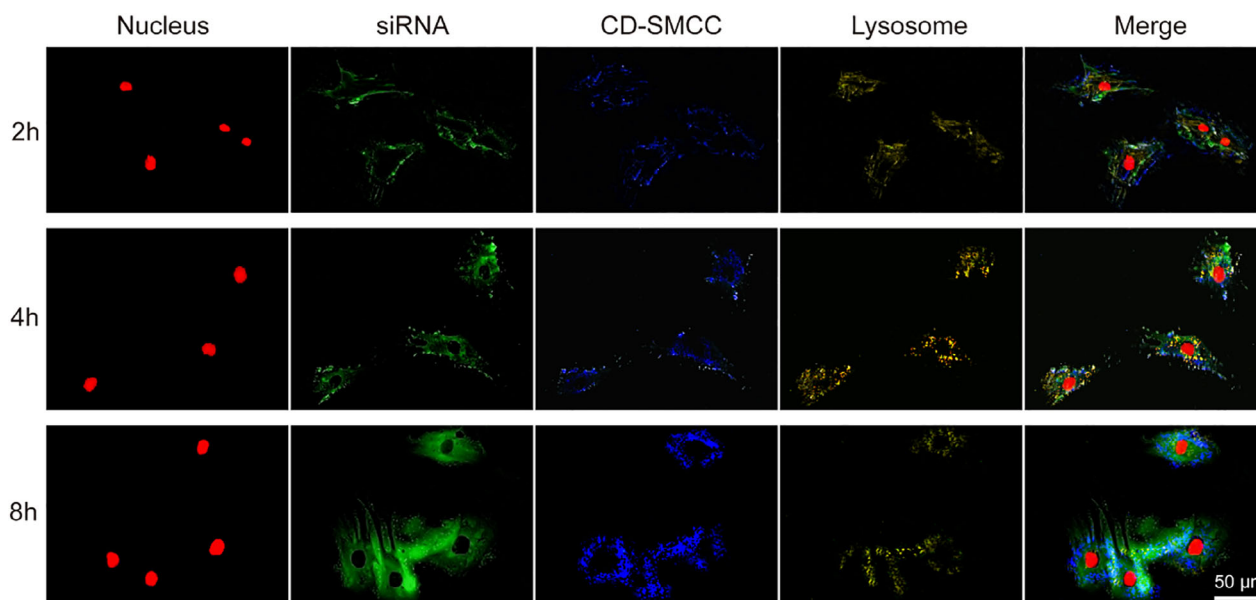
Figure 4. Confocal laser scanning microscope (CLSM) image of carbon dot (CD)-succinimidyl-4-(N-maleimidomethyl) cyclohexane-1-carboxylate (SMCC) bundled small interfering RNA into mesenchymal stem cells (red fluorescence: RedDod1-labeled nuclei, green fluorescence: FAM-siTnfα, blue fluorescence: CD-SMCC, endosomes and lysosomes were labeled in yellow with LysoTracker TM yellow). Scale bar: 50 μm.

Gene Silencing Efficiency of CD-SMCC-si*Tnfα*

A real-time PCR assay was performed to evaluate the gene silencing efficiency of CD-SMCC-si*Tnfα* complexes at the mRNA level. As shown in Figure 5B, mRNA expression levels of *Tnfα* exhibited a time-dependent increase in each group. No significant differences were found between the untreated MSCs and CD-SMCC groups. Compared with the untreated MSCs, the expression of *Tnfα* was markedly downregulated in both the PEI-si*Tnfα* (PEI-Si) and CD-SMCC-si*Tnfα* transfected MSC (CD-SMCC-Si) groups at each time point ($p < .05$). Significantly lower gene expression was shown in CD-SMCC-Si than that in the PEI-Si group ($p < .05$), with the gap deepening in a time-dependent manner. The results indicate that CD-SMCC may better prevent siRNA from enzymatic degradation and guarantee the effective delivery of siRNA to the cytoplasm compared with commercial PEI, which is beneficial to improving the efficiency of gene silencing. In particular, the effect of gene silencing becomes more pronounced after a long period of transfection.

Suppression of Tnfα by CD-SMCC-si*Tnfα* Promoted GAG Production in MSCs

To further investigate the effect of *Tnfα* silencing by transfection of CD-SMCC-si*Tnfα* with an optimized dose on chondrogenic differentiation of MSCs, we measured GAG secretion given as a ratio of GAG to DNA content by biochemical assays after 7, 14, and 21 days. As shown in Figure 5C, the DNA content exhibited a time-dependent increase in each group, which suggested that the numbers of cells increased with time. During the process, there was no significant difference among the DNA content in the untreated, CD-SMCC and CD-SMCC-Si groups ($p > .05$), indicating that CD-SMCC has negligible toxicity. In contrast, the DNA content of the PEI-Si group was significantly decreased after 14 days ($p < .05$), showing slight cytotoxicity of PEI.

GAG content showed an increase in a time-dependent manner in the CD-SMCC-Si and PEI-Si groups, which changed little with time in the untreated and CD-SMCC groups (Fig. 5D). Compared with the untreated group, the GAG content rapidly increased in the CD-SMCC-Si group after 7 days, whereas it increased in the PEI-Si group after 14 days. At each time point, the GAG content was significantly higher in the CD-SMCC-Si group than that in the PEI-Si group ($p < .05$). Particularly, the GAG secretion of the CD-SMCC-Si group was 1.87-, 2.8-, and 5.05-fold higher than that in the untreated group at 7, 14 and 21 days, respectively ($p < .05$). These findings demonstrated that the interference of *Tnfα* in MSCs by CD-SMCC-si*Tnfα* transfection promotes chondrogenic differentiation by increasing the production of GAG, which is a marker of cartilage matrix.

Tnfα Silencing by CD-SMCC-si*Tnfα* Upregulated the Expression of Cartilage-Specific Genes in MSCs

To detect the effect of *Tnfα* silencing by CD-SMCC-si*Tnfα* transfection on the chondrogenic potential of MSCs at the mRNA level, we used RT-PCR to evaluate the expression of chondrogenic-specific genes including *Sox9*, *Col2a1*, and *Acan*. As shown in Figure 5E–5G, there was a slight time-dependent increase in the mRNA expression levels of these genes in the untreated MSC (untreated) and CD-SMCC transfected MSC (CD-SMCC) groups, whereas there was a sharp increase with time in the PEI-si*Tnfα* (PEI-Si) and CD-SMCC-si*Tnfα* transfected MSC (CD-SMCC-Si) groups. Among all the groups, the CD-SMCC-Si group showed the highest expression level at each time point ($p < .05$, Fig. 5E–5G). Except at day 7, the expression of chondrogenic-specific genes in the CD-SMCC-Si group was significantly higher than that in the PEI-Si group. The results indicate that the high transfection efficiency and biosafety of CD-SMCC-si*Tnfα* contribute to the potent silencing effect, which further promotes the chondrogenic potential of MSCs by immune modulation. It has been reported that the pro-inflammatory responses of MSCs were inhibited by using the intracellular release of a small-molecule inhibitor of NF-kB
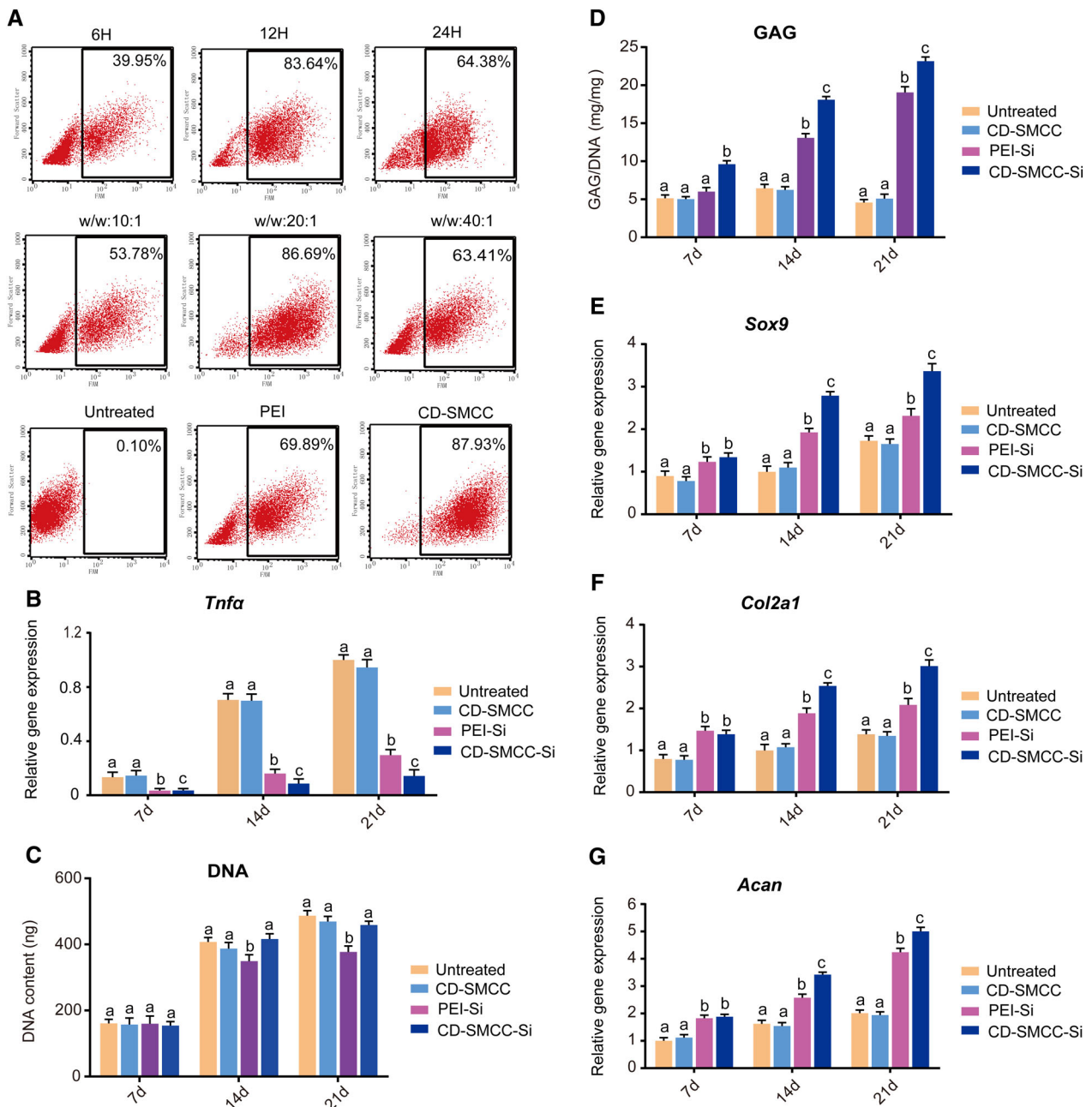
Figure 5. Flow cytometric and real time (RT)-PCR analyses of Tnfα gene transfection and silencing efficiency. **(A):** Flow cytometry was performed to characterize the quantitative determination of FAM-siTnfα-positive transfected mesenchymal stem cells (MSCs) for various times, different weight ratios and transfection reagents. **(B):** RT-PCR analysis of Tnfα mRNA levels in the MSCs following treatment with the different transfection reagents for 7 days, 14 days, and 21 days. **(C):** Cell proliferation was detected based on the DNA content following treatment with the different transfection reagents for 7 days, 14 days, and 21 days. **(D):** The GAG content was measured to assess the biosynthetic activity. **(E–G):** RT-PCR analysis of Sox9, Col2a1, and Acan mRNA levels in the MSCs following treatment with the different transfection reagents for 7 days, 14 days, and 21 days. The bars with different letters (a, b, c) of each time point are significantly different from each other at $p < .05$.

by microparticles [38]. As NF-kB can be upregulated by TNFα in MSCs [39, 40], inhibition of *Tnfα* may be a potential target for gene therapy of cartilage defects [10, 41].

Enhanced Therapeutic Effect of CD-SMCC-si*Tnfα* Transfected MSCs on Cartilage Regeneration

Numerous studies have demonstrated that TNFα induces chondrocyte apoptosis and prevents cartilage matrix synthesis (e.g.,

aggrecan and type II collagen) [12, 42]. Conversely, inhibition of TNFα can repair the degeneration of the cartilage matrix [43]. Therefore, we hypothesized that knockdown of *Tnfα* may contribute to the acceleration of cartilage regeneration. To validate our hypothesis, MSCs transfected with CD-SMCC-si*Tnfα* and PEI-si*Tnfα* were implanted into a cartilage defect model, along with a control. The conditions of all rats were almost the same before and after the surgery. All rats were included in the analysis below. Upon
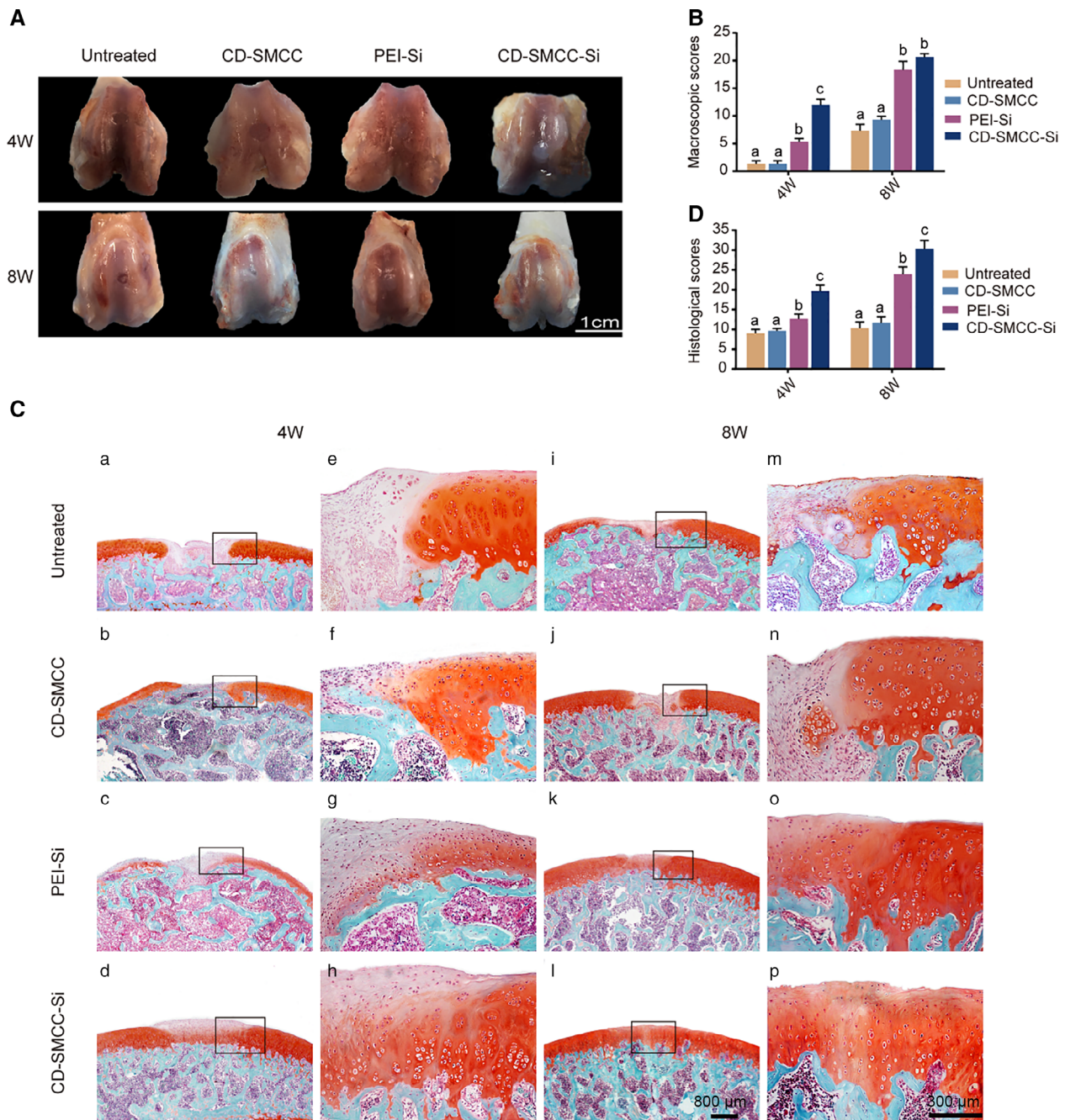
Figure 6. Macroscopic assessment of articular cartilage defects, International Cartilage Repair Society score, Safranin-O staining, and histological evaluation. **(A):** Macroscopic assessment of the cartilage defect repair in the four groups at different times after surgery. **(B):** Macroscopic score of the cartilage defect repair at 4 weeks and 8 weeks. **(C):** Safranin-O staining of the cartilage defect healing at 4 weeks **(Ca–Ch)** and 8 weeks **(Ci–Cp)**. (Ca–Cd) and (Ci–Cl)—scale bar: 800 μm. (Ce–Ch) and (Cm–Cp): magnification of black frame selected area (scale bar: 300 mm). **(D):** Histological score of the cartilage defect repair at 4 weeks and 8 weeks. The bars with different letters (a, b, c) in (B) and (D) at each time point indicate $p < .05$.

macroscopic observation, no infection, malformation, or severe synovitis was present in the engineered cartilage in all the groups (Fig. 6A). Four weeks post-transplantation, defects in the untreated and CD-SMCC (empty vector treated) groups were blank with little tissue. In contrast, glossy white regenerated tissues integrated with the surrounding tissues were observed in the defects of the CD-SMCC-Si and PEI-Si groups. Particularly, part of the neo-tissue in the CD-SMCC-Si group was almost indistinguishable from the surrounding tissue. Eight weeks after

the operation, the defects in the control and CD-SMCC group were filled with a thin and irregular layer of fibrous tissue discernible from the surrounding tissues. In the CD-SMCC-Si and PEI-Si groups, the defects were mostly filled with opaque white cartilage-like tissue well integrated with the surrounding tissues. For the CD-SMCC-Si group, the margin between the neo-tissue and the original cartilage could hardly be discerned. The score of ICRS further confirmed the macroscopic evaluation. At each time point, the CD-SMCC-Si group scored the highest and was
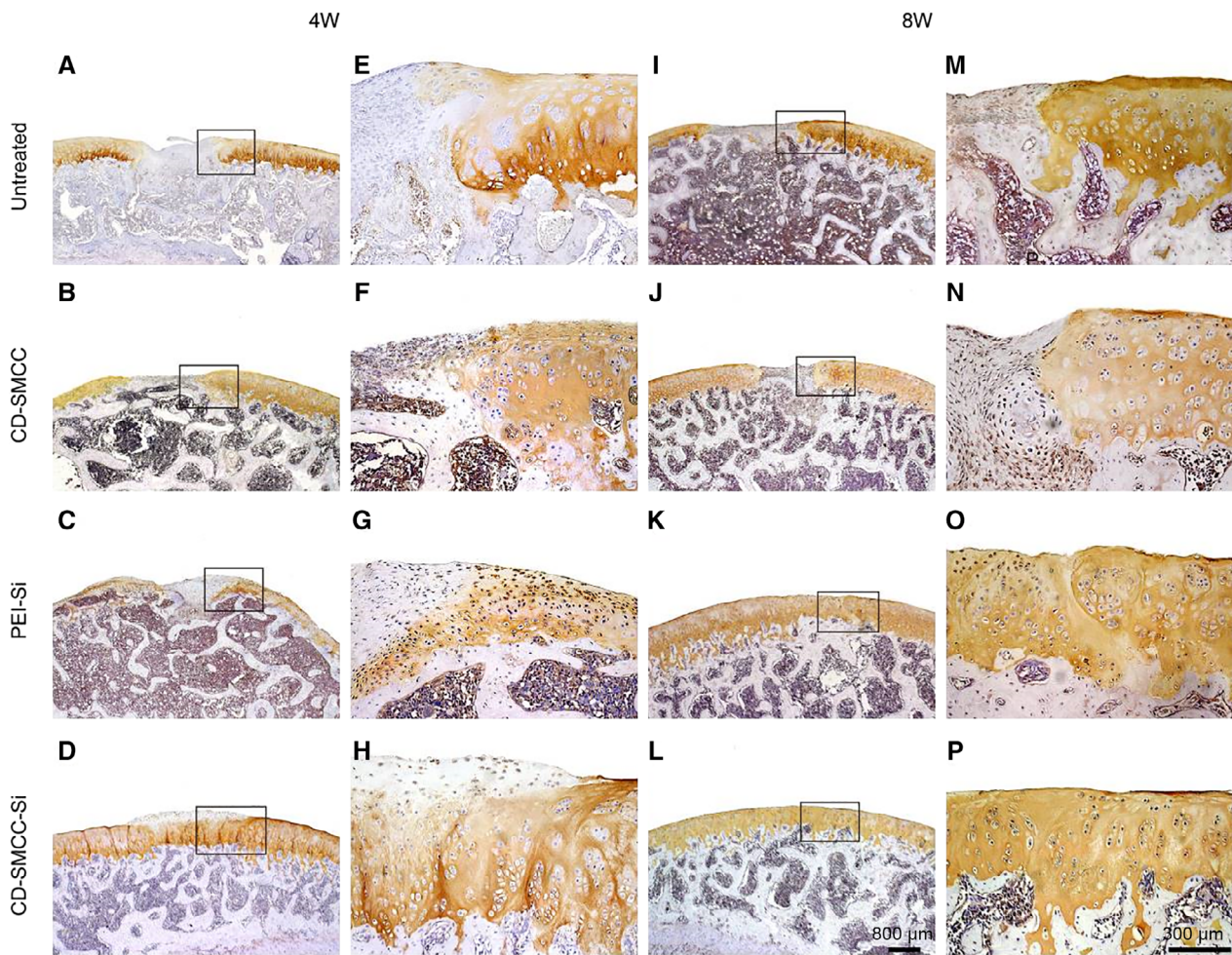
Figure 7. Type II collagen immunohistological staining of the cartilage defect healing at 4 weeks **(A–H)** and 8 weeks **(I–P)**. (A–D) and (I–L)—scale bar: 800 μm. (E–H) and (M–P) magnification of black frame selected area (scale bar: 300 mm).

followed by the PEI-Si group, both of which were much higher than the untreated and CD-SMCC groups (Fig. 6B).

To further confirm the effect of cartilage repair, histological evaluation of specimens was carried out. At 4 or 8 weeks after operation, H&E staining analysis (Supporting Information Fig. S1) and Safranin-O staining showed that the defects on the joint surface in untreated (Fig. 6Ca, 6Ce, 6Ci, 6Cm) and CD-SMCC groups (Fig. 6C, 6Cb, 6Cf, 6Cj, 6Cn) were unfavorably repaired and were filled with mainly inflammatory cells, with a small amount of fibrous tissue. In addition, the boundary between the neo-tissue and the original cartilage tissue was clearly distinguishable in the two groups. Identified by Safranin-O, negative staining was shown in the defect of untreated (Fig. 6Ca, 6Ce, 6Ci, 6Cm) and CD-SMCC groups (Fig. 6Cb, 6Cf, 6Cj, 6Cn). Conversely, the newly regenerated tissue progressed from fibrous cartilage-like to hyaline cartilage-like tissue in both PEI-Si (Fig. 6Cc, 6Cg, 6Ck, 6Co) and CD-SMCC-Si groups (Fig. 6Cd, 6Ch, 6Cl, 6Cp). In addition, modicum inflammatory cells were dispersed in the defect at 4 weeks. Round chondrocytic cells embedded in the lacuna, a typical feature of hyaline cartilage, were observed in the defect after 8 weeks of therapy (Fig. 6Ck, 6Cl, 6Co, 6Cp). Safranin-O staining also showed positive staining that intensified with time, indicating a time-dependent accumulation of proteoglycans, which are markers of the cartilage matrix. In the CD-SMCC-Si group, the most abundant matrix was

shown in the defect, with an interface that was hardly distinguishable (Fig. 6Cl, 6Cp) from the surrounding tissue. Histological scores further validated the observation at different times, in the order of CD-SMCC-Si, PEI-Si and untreated/CD-SMCC (Fig. 6D). The CD-SMCC group scored almost the same as the untreated group, not only in the macroscopic evaluation but also in the histological assay, which demonstrated the safety of CD-SMCC.

Immunohistochemical staining for type II collagen specific to the cartilage matrix showed intense positive staining (brown) in the regenerated tissue of the PEI-Si and CD-SMCC-Si groups and negative staining in those of the untreated and CD-SMCC groups. Stronger staining of COL2A1 was observed in the CD-SMCC-Si group compared with the others, indicating the most deposited cartilage matrix (Fig. 7D).

Reduced Inflammation by Therapy of CD-SMCC-si*Tnfα* Transfected MSCs

For MSC-based therapy, the therapeutic efficacy of MSCs is often impaired by inflammation [44, 45], in which TNFα plays a crucial role. Our immunohistochemical findings showed intense positive staining of TNFα during the process of therapy by MSCs (untreated group), indicating the occurrence of inflammation (Supporting Information Fig. S2A, S2C, S2E, S2G). However, after introduction of CD-SMCC-si*Tnfα* transfection,

the expression of TNFα was markedly inhibited (Supporting Information Fig. S2B, S2D, S2F, S2H), as evidenced by almost negative staining. The results were negatively correlated with the expression of type II collagen, demonstrating that TNFα may be an inhibitor in chondrogenic differentiation. Thus, suppression of TNFα promotes chondrogenic differentiation by inhibition of host inflammation, favorable for cartilage regeneration.

CONCLUSION

In summary, this is the first study to report novel multifunctional and highly biocompatible CD-SMCC nanoparticles as a gene carrier to transfer si*Tnfα* into MSCs in an attempt to promote chondrogenic differentiation. CD-SMCC had favorable biocompatibility, low toxicity, high transfection efficiency and excellent complexing ability with siRNA, which is preferred over the commercial transfection reagent, PEI25k. In addition, it was observed that the silencing of TNFα (si*Tnfα*) in MSCs markedly promoted the chondrogenic differentiation of MSCs and further accelerated cartilage regeneration in vivo. This work may suggest potential for the application of gene therapy in cartilage tissue engineering.

AUTHOR CONTRIBUTIONS

J.Z., M.H.: designed the study, final approval of manuscript; L.Z.: designed the study, prepared the draft of the manuscript, final approval of manuscript; X.Z.: guided the work, final approval of manuscript; J.L.: conducted the assays, collected the statistics, prepared the draft of the manuscript, final approval of manuscript; T.J.: conducted the assays, prepared the draft of the manuscript, final approval of manuscript; C.L.: conducted the assays, final approval of manuscript; Y.W.: conducted the assays, collected the statistics, final approval of manuscript.

DISCLOSURE OF POTENTIAL CONFLICTS OF INTEREST

The authors indicated no potential conflicts of interest.

DATA AVAILABILITY STATEMENT

The data that support the findings of this study are available from the corresponding author upon reasonable request.

REFERENCES

1 Li D, Cheng P, Jiang H et al. Vascularization converts the lineage fate of bone mesenchymal stem cells to endothelial cells in tissue-engineered bone grafts by modulating FGF2-RhoA/ROCK signaling. Cell Death Dis 2018;9:959.

2 Lalu MM, Mazzarello S, Zlepnig J et al. Safety and efficacy of adult stem cell therapy for acute myocardial infarction and ischemic heart failure (SafeCell Heart): A systematic review and meta-analysis. STEM CELLS TRANSLATIONAL MEDICINE 2018;7:857–866.

3 Jiang T, Kai D, Liu S et al. Mechanically cartilage-mimicking poly(PCL-PTHF urethane)/collagen nanofibers induce chondrogenesis by blocking NF-kappa B signaling pathway. Biomaterials 2018;178:281–292.

4 Navas A, Magana-Guerrero FS, Dominguez-Lopez A et al. Anti-inflammatory and anti-fibrotic effects of human amniotic membrane mesenchymal stem cells and their potential in corneal repair. STEM CELLS TRANSLATIONAL MEDICINE 2018;7:906–917.

5 Lin T, Pajarinen J, Nabeshima A et al. Establishment of NF-kappaB sensing and interleukin-4 secreting mesenchymal stromal cells as an "on-demand" drug delivery system to modulate inflammation. Cytotherapy 2017;19:1025–1034.

6 Oishi Y, Manabe I. Macrophages in inflammation, repair and regeneration. Int Immunol 2018;30:511–528.

7 Gu X, Gu B, Lv X et al. 1,25-Dihydroxyvitamin D3 with tumor necrosis factor-alpha protects against rheumatoid arthritis by promoting p53 acetylation-mediated apoptosis via Sirt1 in synoviocytes. Cell Death Dis 2016;7:e2423.

8 Korb-Pap A, Stratis A, Muhlenberg K et al. Early structural changes in cartilage and bone are required for the attachment and invasion of inflamed synovial tissue during destructive inflammatory arthritis. Ann Rheum Dis 2012;71:1004–1011.

9 Kaneko K, Williams RO, Dransfield DT et al. Selective inhibition of membrane type 1 matrix metalloproteinase abrogates progression of experimental inflammatory arthritis: Synergy with tumor necrosis factor blockade. Arthritis & Rheumatol 2016;68:521–531.

10 Wehling N, Palmer GD, Pilapil C et al. Interleukin-1beta and tumor necrosis factor alpha inhibit chondrogenesis by human mesenchymal stem cells through NF-kappaB-dependent pathways. Arthritis Rheum 2009;60:801–812.

11 Sitcheran R, Cogswell PC, Baldwin AS Jr. NF-kappaB mediates inhibition of mesenchymal cell differentiation through a posttranscriptional gene silencing mechanism. Genes Dev 2003;17:2368–2373.

12 Lopez-Armada MJ, Carames B, Lires-Dean M et al. Cytokines, tumor necrosis factor-alpha and interleukin-1beta, differentially regulate apoptosis in osteoarthritis cultured human chondrocytes. Osteoarthr Cartil 2006;14:660–669.

13 Joos H, Wildner A, Hogrefe C et al. Interleukin-1 beta and tumor necrosis factor alpha inhibit migration activity of chondrogenic progenitor cells from non-fibrillated osteoarthritic cartilage. Arthritis Res Ther 2013;15:R119.

14 Tang Q, Hao L, Peng Y et al. RNAi silencing of IL-1beta and TNF-alpha in the treatment of post-traumatic arthritis in rabbits. Chem Biol Drug Des 2015;86:1466–1470.

15 Paquet J, Henrionnet C, Pinzano A et al. Alternative for anti-TNF antibodies for arthritis treatment. Mol Ther 2011;19:1887–1895.

16 Yah CS, Simate GS, Iyuke SE. Nanoparticles toxicity and their routes of exposures. Pak J Pharm Sci 2012;25:477–491.

17 Yang X, Wang Y, Shen X et al. One-step synthesis of photoluminescent carbon dots with excitation-independent emission for selective bioimaging and gene delivery. J Colloid Interface Sci 2017;492:1–7.

18 Zhou J, Deng W, Wang Y et al. Cationic carbon quantum dots derived from alginate for gene delivery: One-step synthesis and cellular uptake. Acta Biomater 2016;42:209–219.

19 Wu Y, Zhou B, Xu F et al. Functional quantum dot-siRNA nanoplexes to regulate chondrogenic differentiation of mesenchymal stem cells. Acta Biomater 2016;46:165–176.

20 Tsoi KM, Dai Q, Alman BA et al. Are quantum dots toxic? Exploring the discrepancy

between cell culture and animal studies. Acc Chem Res 2013;46:662–671.

21 Shao D, Lu M, Xu D et al. Carbon dots for tracking and promoting the osteogenic differentiation of mesenchymal stem cells. Biomater Sci 2017;5:1820–1827.

22 Wang L, Wang X, Bhirde A et al. Carbon-dot-based two-photon visible nanocarriers for safe and highly efficient delivery of siRNA and DNA. Adv Healthc Mater 2014;3:1203–1209.

23 Pereira M, Lai EP. Capillary electrophoresis for the characterization of quantum dots after non-selective or selective bioconjugation with antibodies for immunoassay. J Nanobiotechnol 2008;6:10.

24 Li F, Wang Z, Huang Y et al. Delivery of PUMA apoptosis gene using polyethyleneimine-SMCC-TAT/DNA nanoparticles: Biophysical characterization and in vitro transfection into malignant melanoma cells. J Biomed Nanotechnol 2015;11:1776–1782.

25 Guo Y, Werbel T, Wan S et al. Potent antigen-specific immune response induced by infusion of spleen cells coupled with succinimidyl-4-(N-maleimidomethyl cyclohexane)-1-carboxylate (SMCC) conjugated antigens. Int Immunopharmacol 2016;31:158–168.

26 Jiang T, Xu G, Wang Q et al. In vitro expansion impaired the stemness of early passage mesenchymal stem cells for treatment of cartilage defects. Cell Death Dis 2017;8:e2851.

27 Farndale RW, Buttle DJ, Barrett AJ. Improved quantitation and discrimination of sulphated glycosaminoglycans by use of dimethylmethylene blue. Biochim Biophys Acta 1986;883:173–177.

28 van den Borne MP, Raijmakers NJ, Vanlauwe J et al. International Cartilage Repair Society (ICRS) and Oswestry macroscopic cartilage evaluation scores validated for use in Autologous Chondrocyte Implantation (ACI) and microfracture. Osteoarthr Cartil 2007;15:1397–1402.

29 Guo X, Park H, Young S et al. Repair of osteochondral defects with biodegradable hydrogel composites encapsulating marrow mesenchymal stem cells in a rabbit model. Acta Biomater 2010;6:39–47.

30 Liu C, Zhang P, Zhai X et al. Nano-carrier for gene delivery and bioimaging based on carbon dots with PEI-passivation enhanced fluorescence. Biomaterials 2012;33:3604–3613.

31 Das S, Debnath N, Cui Y et al. Chitosan, carbon quantum dot, and silica nanoparticle mediated dsRNA delivery for gene silencing in *Aedes aegypti*: A comparative analysis. ACS Appl Mater Interfaces 2015;7:19530–19535.

32 Li S, Liu Z, Ji F et al. Delivery of quantum dot-siRNA nanoplexes in SK-N-SH cells for BACE1 gene silencing and intracellular imaging. Mol Ther Nucl Acids 2012;1:e20.

33 Wang Z, Liu G, Zheng H et al. Rigid nanoparticle-based delivery of anti-cancer siRNA: Challenges and opportunities. Biotechnol Adv 2014;32:831–843.

34 Layzer JM, McCaffrey AP, Tanner AK et al. In vivo activity of nuclease-resistant siRNAs. RNA 2004;10:766–771.

35 Nguyen DN, Mahon KP, Chikh G et al. Lipid-derived nanoparticles for immunostimulatory RNA adjuvant delivery. Proc Natl Acad Sci USA 2012;109:E797–E803.

36 Pouton CW, Seymour LW. Key issues in non-viral gene delivery. Adv Drug Deliv Rev 2001;46:187–203.

37 Chen J, Wang Q, Zhou J et al. Porphyra polysaccharide-derived carbon dots for non-viral co-delivery of different gene combinations and neuronal differentiation of ectodermal mesenchymal stem cells. Nanoscale 2017;9:10820–10831.

38 Ranganath SH, Tong Z, Levy O et al. Controlled inhibition of the mesenchymal stromal cell pro-inflammatory secretome via microparticle engineering. Stem Cell Rep 2016;6:926–939.

39 Carrero R, Cerrada I, Lledo E et al. IL1beta induces mesenchymal stem cells migration and leucocyte chemotaxis through NF-kappaB. Stem Cell Rev 2012;8:905–916.

40 Lee MJ, Kim J, Kim MY et al. Proteomic analysis of tumor necrosis factor-alpha-induced secretome of human adipose tissue-derived mesenchymal stem cells. J Proteome Res 2010;9:1754–1762.

41 Jagielski M, Wolf J, Marzahn U et al. The influence of IL-10 and TNFalpha on chondrogenesis of human mesenchymal stromal cells in three-dimensional cultures. Int J Mol Sci 2014;15:15821–15844.

42 Liu X, Xu Y, Chen S et al. Rescue of proinflammatory cytokine-inhibited chondrogenesis by the antiarthritic effect of melatonin in synovium mesenchymal stem cells via suppression of reactive oxygen species and matrix metalloproteinases. Free Radic Biol Med 2014;68:234–246.

43 Wu CC, Chen WH, Zao B et al. Regenerative potentials of platelet-rich plasma enhanced by collagen in retrieving pro-inflammatory cytokine-inhibited chondrogenesis. Biomaterials 2011;32:5847–5854.

44 Darlington PJ, Boivin MN, Renoux C et al. Reciprocal Th1 and Th17 regulation by mesenchymal stem cells: Implication for multiple sclerosis. Ann Neurol 2010;68:540–545.

45 Kuang W, Zheng L, Xu X et al. Dysregulation of the miR-146a-Smad4 axis impairs osteogenesis of bone mesenchymal stem cells under inflammation. Bone Res 2017;5:17037.

See www.StemCellsTM.com for supporting information available online.